ARMY RESEARCH LABORATORY

Design and Processing of Structural Composite Batteries

**by E. L. Wong, D. M. Baechle, K. Xu, R. H. Carter,
J. F. Snyder, and E. D. Wetzel**

ARL-RP-194 **September 2007**

A reprint from the *Proceedings of Society for the Advancement of Materiel and Process Engineering (SAMPE) 2007 Symposium and Exhibition,* Baltimore, Maryland, 3–7 June 2007.

NOTICES

Disclaimers

The findings in this report are not to be construed as an official Department of the Army position unless so designated by other authorized documents.

Citation of manufacturer's or trade names does not constitute an official endorsement or approval of the use thereof.

Destroy this report when it is no longer needed. Do not return it to the originator.

Army Research Laboratory
Aberdeen Proving Ground, MD 21005-5069

ARL-RP-194 **September 2007**

Design and Processing of Structural Composite Batteries

by E. L. Wong, D. M. Baechle, K. Xu, R. H. Carter,
J. F. Snyder, and E. D. Wetzel
U.S. Army Research Laboratory
Weapons and Materials Research Directorate

A reprint from the *Proceedings of Society for the Advancement of Materiel and Process Engineering (SAMPE) 2007 Symposium and Exhibition,* Baltimore, Maryland, 3–7 June 2007.

REPORT DOCUMENTATION PAGE

Form Approved
OMB No. 0704-0188

1. REPORT DATE *(DD-MM-YYYY)*	**2. REPORT TYPE**	**3. DATES COVERED (From - To)**
September 2007	Reprint	

4. TITLE AND SUBTITLE
Design and Processing of Structural Composite Batteries

5a. CONTRACT NUMBER

5b. GRANT NUMBER

5c. PROGRAM ELEMENT NUMBER

6. AUTHOR(S)
E. L. Wong, D. M. Baechle, K. Xu, R. H. Carter, J. F. Snyder, and E. D. Wetzel

5d. PROJECT NUMBER

5e. TASK NUMBER

5f. WORK UNIT NUMBER

7. PERFORMING ORGANIZATION NAME(S) AND ADDRESS(ES)
U.S. Army Research Laboratory
ATTN: AMSRD-ARL-WM-MA
Weapons and Materials Research Directorate,
Aberdeen Proving Ground, MD, 21005-5069.

8. PERFORMING ORGANIZATION REPORT NUMBER
ARL-RP-194

9. SPONSORING/MONITORING AGENCY NAME(S) AND ADDRESS(ES)
U.S. Army Research Laboratory
2800 Powder Mill Road
Adelphi, MD 20783-1197

10. SPONSOR/MONITOR'S ACRONYM(S)

11. SPONSOR/MONITOR'S REPORT NUMBER(S)
ARL-RP-194

12. DISTRIBUTION/AVAILABILITY STATEMENT
Approved for public release; distribution is unlimited.

13. SUPPLEMENTARY NOTES

14. ABSTRACT

This report is a reprint from the *Proceedings of Society for the Advancement of Materiel and Process Engineering (SAMPE) 2007 Symposium and Exhibition* held in Baltimore, MD, on 3–7 June 2007
Multifunctional structural composites are being developed to simultaneously bear mechanical loads and store electrochemical energy. These composite batteries can replace inert structural components and concurrently provide supplementary power for light load applications. Significant weight savings can be achieved by designing composite battery components, packaging, electrolyte, separator, and/or electrodes with built-in structural and energy efficiency. Prior efforts have focused only on utilizing structural packaging with traditional battery components. In this approach, novel electrolyte and electrode materials are being developed to optimize both electrochemical and mechanical properties. Solvent-free structural vinyl ester polymer electrolytes are being formulated to achieve necessary mechanical strength while enabling ion conductivity. Structural carbon anodes and cathode materials deposited on metal substrates are being developed as electrode components. Charge/discharge cycling is used to evaluate electrochemical capacity of the electrode materials, and tensile tests are used to evaluate their mechanical properties. Several different structural separator materials are being investigated as well. All of these components allow the use of moldable, scalable, and cost-effective composite processing techniques. Progress in the development of each component, and its impact on the overall multifunctional composite battery's electrochemical and mechanical properties will be discussed.

15. SUBJECT TERMS
Fiber metal laminate, battery systems, carbon fiber composites

16. SECURITY CLASSIFICATION OF:			**17. LIMITATION OF ABSTRACT**	**18. NUMBER OF PAGES**	**19a. NAME OF RESPONSIBLE PERSON**
a. REPORT	**b. ABSTRACT**	**c. THIS PAGE**			James F. Snyder
U	U	U	SAR	20	**19b. TELEPHONE NUMBER** (*Include area code*) (410) 306-0842

Standard Form 298 (Rev. 8/98)
Prescribed by ANSI Std. Z39.18

DESIGN AND PROCESSING OF STRUCTURAL COMPOSITE BATTERIES

E. L. Wong[1], D. M. Baechle[1], K. Xu[2], R. H. Carter[1], J. F. Snyder[1]and E. D. Wetzel[1]
[1]U. S. Army Research Laboratory, Weapons and Materials Research Directorate, APG, MD 21005
[2]U. S. Army Research Laboratory, Sensors and Electron Devices Directorate, Adelphi, MD 20783

ABSTRACT

Multifunctional structural composites are being developed to simultaneously bear mechanical loads and store electrochemical energy. These composite batteries can replace inert structural components and concurrently provide supplementary power for light load applications. Significant weight savings can be achieved by designing composite battery components, packaging, electrolyte, separator, and/or electrodes with built-in structural and energy efficiency. Prior efforts have focused only on utilizing structural packaging with traditional battery components. In this approach, novel electrolyte and electrode materials are being developed to optimize both electrochemical and mechanical properties. Solvent-free structural vinyl ester polymer electrolytes are being formulated to achieve necessary mechanical strength while enabling ion conductivity. Structural carbon anodes and cathode materials deposited on metal substrates are being developed as electrode components. Charge/discharge cycling is used to evaluate electrochemical capacity of the electrode materials, and tensile tests are used to evaluate their mechanical properties. Several different structural separator materials are being investigated as well. All of these components allow the use of moldable, scalable, and cost-effective composite processing techniques. Progress in the development of each component, and its impact on the overall multifunctional composite battery's electrochemical and mechanical properties will be discussed.

KEY WORDS: Fiber metal laminate, battery systems, carbon fiber composites

1. INTRODUCTION

For some engineering systems, batteries comprise a significant fraction of the overall system mass and volume. Examples include small, battery powered unmanned aerial vehicles, and automobiles with hybrid battery-combustion powerplants. The performance of these systems can be improved by minimizing overall weight and volume, while maximizing available energy and power. One way to address this challenge is to improve battery energy density. A different approach is to create a structural composite battery (1, 2, 3), where a load-bearing structural composite battery is integrated into the body structure and used as a secondary power source. The load-bearing capacity of the structural battery allows it to replace traditional structural materials, thereby reducing overall system mass. Existing studies on structural batteries have mainly focused on creating structural packaging (2).

This paper investigates structural composite batteries in which the fundamental battery components, such as electrodes, electrolyte, and separators, are the primary load-bearing components. These designs have the potential for higher multifunctional performance than batteries that rely primarily on structural packaging.

Our structural battery is a fiber-matrix composite with each component designed for both structural and electrochemical performance. The design utilizes a carbon fiber anode, cathode material cast on a metal substrate, glass fiber separator, and a polymer electrolyte matrix. The carbon anode and cathode substrate serve as current collectors and are designed to be load-bearing. The structural polymer electrolyte conducts lithium ions between the anode and cathode to participate in the electrochemical reactions as the battery charges/discharges, while transferring mechanical load to the reinforcing anode, cathode, and separator layers. The electrolyte also provides an electrically insulative barrier between the electrodes. Lithium-ion chemistry was chosen for this composite battery due to its high energy density and compatibility with polymer electrolytes (6). This design has the potential for weight and volume reductions which would improve performance in many applications.

Most attempts to create structural electrolytes result in materials with ionic conductivities that are lower than conventional polymer electrolytes (4, 5). Therefore, for our high impedance electrolytes, the distance between the electrodes limits the rate of charges/discharges of the battery. To minimize this electrolyte spacing, a porous separator is used to ensure a constant electrolyte thickness and prevent electrode short-circuiting. For our multifunctional battery, a glass fiber fabric is used as the separator. This separator material provides both electrical isolation and structural support to the composite battery.

Previous efforts have emphasized the electrochemical properties of the individual composite components (4, 5). This paper focuses on the mechanical design and characterization of the structural composite battery. Material selection and the mechanical impact of these materials on overall composite performance are discussed. Mechanical tests are performed on the cathode substrates, anode materials, and full battery composites. A linear elastic model of the battery composite will be presented and compared with the results of composite battery mechanical testing.

2. EXPERIMENTAL

2.1 Materials

2.1.1 Electrolyte Previous accounts detailed our evolution of vinyl ester resins for use as structural electrolytes (4). Here, a single electrolyte formulation is used exclusively to simplify the mechanical testing of the structural composite battery. The electrolyte is a vinyl ester random copolymer comprised of 80 wt% methoxy poly(ethylene glycol) 550 monoacrylate and 20 wt% ethoxylated pentaerythritol tetraacrylate. Both components were acquired from Sartomer Company with the respective product numbers CD553 and SR494. Sartomer reports the resin densities to be 1.1 g/cm^3. The bulk electrolyte has been tested to have an ion conductivity of 4×10^{-6} S/cm^2 and a compressive modulus of 25 MPa. (4, 5). Currently, research

is being conducted on other types of electrolytes with better ion conductivities and moduli and will be addressed in future publications.

2.1.2 Anode Two structural anode fabrics were tested: a plain-woven carbon fabric and a non-woven carbon fabric. These fabrics were selected for this study based on their good anodic electrochemical capacity values as measured in previous studies (4, 5, 7). The woven fabric, style 4163 from Textile Products Inc., is a 12.5×13 yarn per inch fabric composed of 3k tows of T-300 carbon fiber. The non-woven fabric is grade 8000036 from Hollingsworth and Vose. Both of these fabrics are shown in Figure 1, and their mechanical and electrochemical properties in the roll direction are summarized in Table 1. The thickness and areal density values are from the manufacturer, and the capacity values were reported previously (5). The non-woven fabric was tested as described in Section 3.1 to provide the stiffness and strength values reported in Table 1. The stiffness and strength values of the woven fabric reported in Table 1 were calculated as described in Section 4.1.

2.1.3 Cathode The composite cathode material utilizes $LiFePO_4$ chemistry. The composition of the cathode material film deposited onto the metal substrate is 72wt% $LiFePO_4$, 8wt% acetylene black, and 20wt% poly(ethylene oxide) 200k as a binder. Acetylene black ensures electrical conductivity throughout the film (8), and the binder keeps the film intact during processing. These materials are solvent cast on the metal substrate using acetonitrile. The measured electrochemical capacity of the active material is 85 mAh/g (4, 5).

Table 1. Structural anode properties. Mechanical properties are reported in the roll direction.

Fabric Style	Thickness (mm)	Areal Density (g/m^2)	Effective Volume Fraction	Capacity (mAh/g)	Specific Tensile Stiffness ($GPa/(g/cm^3)$)	Specific Tensile Strength ($MPa/(g/cm^3)$)
Non-woven	0.25	34	7.6%	117	20.8	87.5
Woven	0.33	202	34%	199	65.3	1100

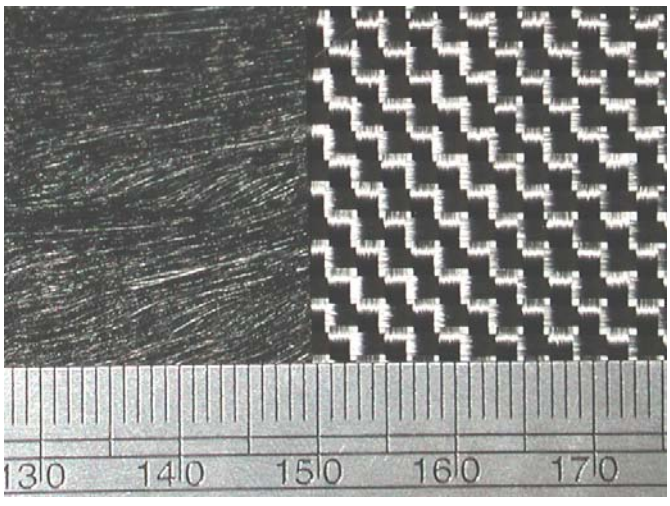

Figure 1. Non-woven (left) and woven (right) structural anodes.

Many different types of metal substrates are chemically stable with $LiFePO_4$ chemistry (over a 2.8-4.0V range (8)) including stainless steel and titanium. Stainless steel was evaluated in this study due to its high availability and low cost. Trends in stainless steel mechanical performance due to sample geometry can be extrapolated to other candidate cathode substrate materials. A solid foil is not suitable because it does not allow through-thickness resin flow during composite processing. Instead, three geometries of porous foil were investigated: a woven mesh, an expanded foil and a perforated foil. The woven (McMaster-Carr part #9656T181) and perforated (McMaster-Carr part #9329T1) foils are composed 304 stainless steel, while the expanded foil (Dexmet part #5SS(316L) 10-050) is composed of 316L stainless steel. These foils' different geometries are shown in Figure 2, and their properties are summarized in Table 2. The stiffness and strength values in Table 2 are roll direction properties. The thickness of the foils range from 0.2 to 0.25 mm, and the effective density varies between geometries. The geometry of the openings can be tailored to the application in the future. The open surface area of all three architectures was chosen to be approximately 30% since this is qualitatively a good compromise between in-plane mechanical stiffness and available open area/surface area for cathode material deposition.

2.1.4 Separator The separator is a 4-harness satin weave glass fiber cloth E-BX from Vector Ply. The fabric is 0.11 mm thick and has an areal density of 99 g/m^2 and approximately 64×64 yarns per inch. The effective fiber volume fraction for this fabric is 35%. Tensile stiffness of this fabric is estimated in Section 4.1. Thinner fabrics are commercially available and will be investigated in the future.

Table 2. Structural cathode properties. Mechanical properties are reported in the roll direction.

Substrate Style	Thickness (mm)	Areal Density (g/m^2)	Effective Volume Fraction	Average Specific Tensile Stiffness ($GPa/(g/cm^3)$)	Average Specific Tensile Strength ($MPa/(g/cm^3)$)
Woven	0.22	596	35%	2.35 ±0.08	38.0 ±0.6
Expanded	0.20	677	42%	1.48 ±0.06	30.6 ±3.5
Perforated	0.25	893	45%	5.74 ±0.28	62.5 ±0.4

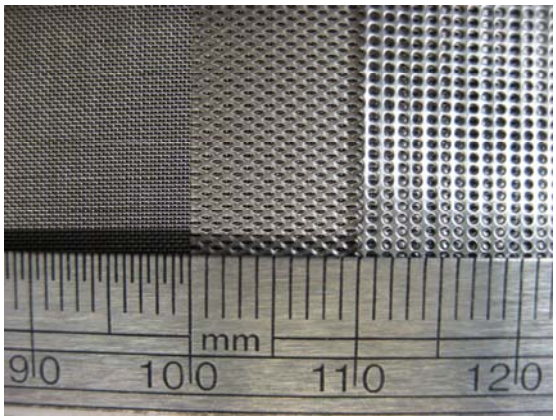

Figure 2. Woven (left), expanded (middle) and perforated (right) stainless steel foils.

2.2 Composite processing Four composite batteries were processed using modified vacuum assisted resin transfer molding (VARTM) to prevent moisture intrusion during fabrication. The general lay-up and fabrication procedure is the same as previously published (4, 5). Two composite batteries were fabricated and tested mechanically, while two other batteries were fabricated and tested electrochemically. Both composite batteries for mechanical testing utilized a woven carbon fabric anode. One of the composites for electrochemical testing utilized a woven carbon fabric anode, while the other composite utilized a non-woven carbon fiber anode. The woven and non-woven carbon anodes are described in section 2.1.2.

All composite batteries utilized the electrolyte described in section 2.1.1, the E-BX glass fiber separator described in section 2.1.4, and the perforated stainless steel cathode substrate and $LiFePO_4$ cathode materials described in Section 2.1.3. The roll direction of the anode, cathode, and separator materials of the composite samples were all oriented along the same axis. Each composite was a double cell consisting of two structural anodes with a cathode sandwiched inbetween. A separator layer was placed in between each anode and cathode interface. A schematic of the composite battery lay-up is shown in Figure 3.

2.3 Mechanical testing All mechanical testing was performed on an MTS Synergie 1000 load frame with a 5 kN load cell, using a constant extension rate of 2.5 mm/min.

2.3.1 Anodes The non-woven fabric was cut into three tensile specimens, each 1.27 cm wide. These samples were clamped in the load frame at a gauge length of 10.2 cm, and tested in tension to failure.

2.3.2 Cathode substrates The active cathode material is granular with no significant mechanical properties, so only the cathode's metal substrate contributes to the mechanical properties of the composite battery. The woven, expanded, and perforated stainless steel foils were tested in tension. In order to test material behavior along different loading directions, samples were cut in different orientations with respect to the roll direction of each material. Three samples were cut for each orientation. The samples were cut in a dogbone shape, as shown in Figure 4. Dimensions and test conditions were chosen to follow the guidelines in ASTM E8-04 (9).

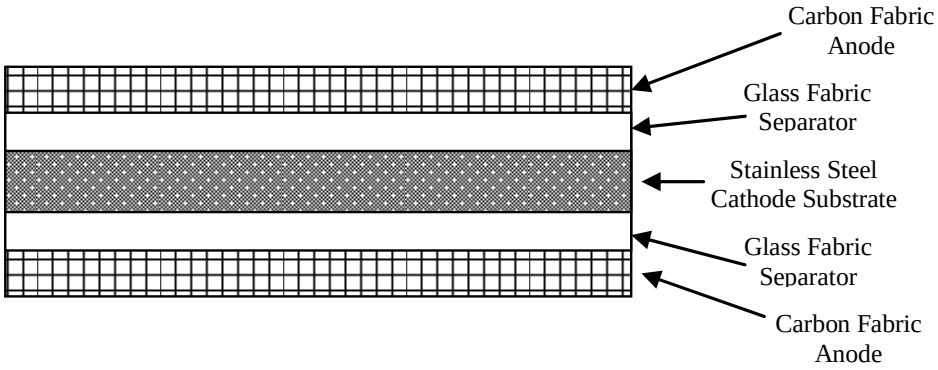

Figure 3. Schematic of the composite battery cross-section.

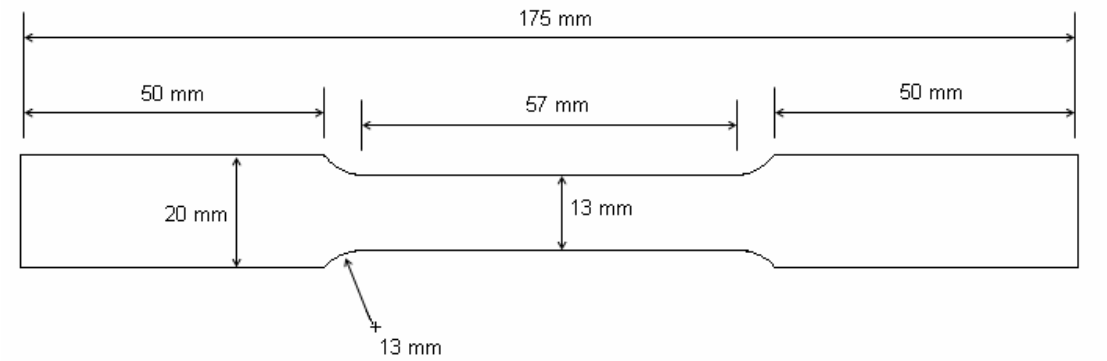

Figure 4. Tensile test specimen schematic.

2.3.3 Composite battery The two composites for mechanical testing were cut into 10 rectangular prismatic strips, each approximately 100 mm long × 13 mm wide × 1 mm thick. The roll direction of the woven carbon fabric (and hence all other plies) was oriented along the test axis. A schematic of the tensile samples' cross-section can be found in Figure 3. After bonding 25 mm long end tabs to each specimen, they were tested in tension.

2.4 Electrochemical testing Electrochemical test procedures and the results of anode and cathode half cells have been reported previously (4, 5). The geometry of the metal is unlikely to affect the electrochemistry of the cathode. The different geometries contribute a different amount of available surface area for cathode material deposition which could affect the energy density, but not the electrochemical capacity or resistance.

2.4.1 Liquid electrolyte full cells For compatibility of electrode materials, an ideal electrolyte and composite electrode components were tested in a coin cell configuration. The ideal electrolyte selected was a liquid electrolyte, 1.0 M $LiPF_6$ in ethylene carbonate/dimethyl carbonate at 30:70 by weight. The structural anode material tested was the non-woven carbon fabric against the $LiFePO_4$ cathode material. Coin cells were tested on a Maccor 4000 at a constant current of $9x10^{-5}$ A during the first three cycles while the SEI layer is being formed (10) and then at $3x10^{-4}$ A for the remainder of the test. Full details on the preparation and procedures to test these coin cells were reported previously (4, 5). In the future, the woven carbon fabric will also be tested in this configuration.

2.4.2 Composite battery Composite batteries were initially screened by using an ohmmeter to measure their anode-to-cathode electrical resistance under dry conditions. In a properly performing battery, this resistance is infinite. The two batteries constructed for this study exhibited finite resistances (Section 4.3), and were not subject to formal electrochemical cycling. Electrochemical cycling of full composite batteries will be reported in a future publication.

3. SUBCOMPONENT TESTING

3.1 Anode mechanical properties In Table 1, the effective volume fractions of the carbon fabrics were calculated by dividing the areal density of each fabric by its thickness, and then normalizing by the density of typical carbon fibers (1.8 g/cm^3). These effective volume fraction values represent the fiber volume fraction that would be expected for a polymer-matrix/carbon-fabric lamina composed of each fabric.

The average measured stiffness and strength values for the non-woven fabric were 2.5 GPa and 10.5 MPa, respectively. These values were then normalized by the areal density and thickness of each fabric type to provide the specific stiffness and strength values reported in Table 1.

Tensile stiffness of the woven fabric was estimated as described in Section 4.1. Strength of the woven fabric was not provided by the manufacturer, but was estimated using the manufacturer's data for the strength of a 3k tow of T-300 carbon fibers, the fiber volume fraction of the fabric, and a simple 0°/90° cross-ply arrangement. Strength and stiffness values for the woven fabric were then divided by the apparent density to provide specific values found in Table 1.

3.2 Cathode mechanical properties Tensile test data revealed the best mechanical configuration of the cathode metal substrate. Elastic modulus was measured by calculating the slope of the stress-strain data points from 0 to 0.2% strain. Some of the specimens exhibited dramatic elongation and change in geometry, so a true stress and strain are reported in Table 3 to account for changing gauge dimensions. Testing of the 45° woven specimens was stopped when the strain exceeded 50%. The corresponding specific stress value would never be reached in this composite battery as the other components would not be able to withstand this amount of strain. The 45° woven samples have a small elastic regime, and yield occurred at around 4 MPa. This low yield point was caused by the woven strands aligning themselves with the test axis as load was applied.

Table 3. Specific true max stress and stiffness of different geometries of stainless steel foil. Orientation refers to test direction relative to roll direction.

Substrate Geometry	**Orientation**	**True Specific Stiffness (GPa/(g/cm^3))**	**True Ultimate Stress (MPa/(g/cm^3))**
Woven	0	2.35 ±0.08	38.0 ±0.6
Woven	90	3.77 ±0.05	43.2 ±2.1
Woven	45	0.28 ±0.02	73.7 ±0.7
Expanded	0	1.48 ±0.06	30.6 ±3.5
Expanded	90	5.52 ±0.39	64.7 ±1.4
Expanded	45	3.35 ±0.45	29.5 ±0.7
Perforated	0	5.74 ±0.28	62.5 ±0.4
Perforated	90	5.74 ±0.28	62.5 ±0.4
Perforated	45	4.05 ±0.40	56.0 ±5.0

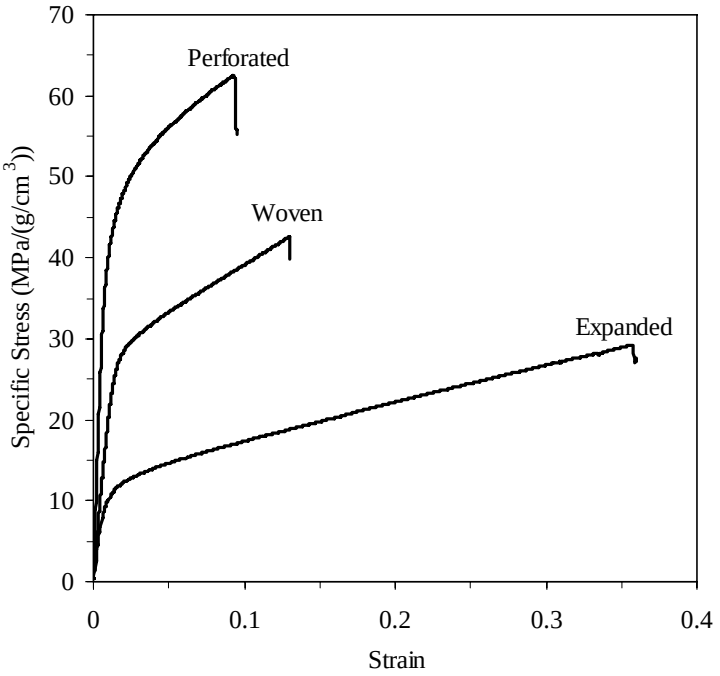

Figure 5. Specific tensile stress vs. strain of different geometries of stainless steel foil. All specimens were oriented along the machine direction.

Figure 5 shows the stress vs. strain behavior along the roll direction of the three stainless steel geometries. These plots illustrate the perforated foil's superior specific stiffness and ultimate stress when compared to the woven and expanded geometries. Tests were not performed on the perforated metals in the 90° direction. The perforations are in a square pattern, thus the behavior at 90° is expected to be close to the material behavior at 0°. As seen in Table 3, the perforated foil has a higher specific stiffness than the expanded and woven metals. The stiffness of the expanded foil in the 90° direction is close to the stiffness of the perforated foil in the same direction, but the perforated foil is stiffer than the expanded foil in the 0° and 45° directions. The specific ultimate stress of the expanded foil is also higher than the perforated foil in the 90° direction. However, the perforated foil is stronger along more loading directions and was determined to be the best mechanical geometry for the cathode substrate.

3.3 Liquid electrolyte full cell In Figure 6, a full cell incorporating the non-woven fabric anode and structural $LiFePO_4$ cathode was cycled for 102 cycles over 63 hours. The charge capacity fades 66% over the first 4 cycles followed by a plateau in which the capacity is reversible. The relatively low capacity in the plateau region, referred to as the reversible capacity, is of some concern. At the fifth cycle, the discharge reversible capacity is 10.00 mAh/g and the charge reversible capacity is 10.04 mAh/g. Since the charge and discharge capacities at and after the fifth cycle are nearly equivalent (as shown in Figure 6b), there is very little irreversible capacity. This equivalency suggests that the non-woven carbon fabric and $LiFePO_4$ are compatible materials and can be used in a structural composite battery. However, the full cell data is preliminary and based on only one trial, therefore further testing is underway to confirm the data and resolve these discrepancies.

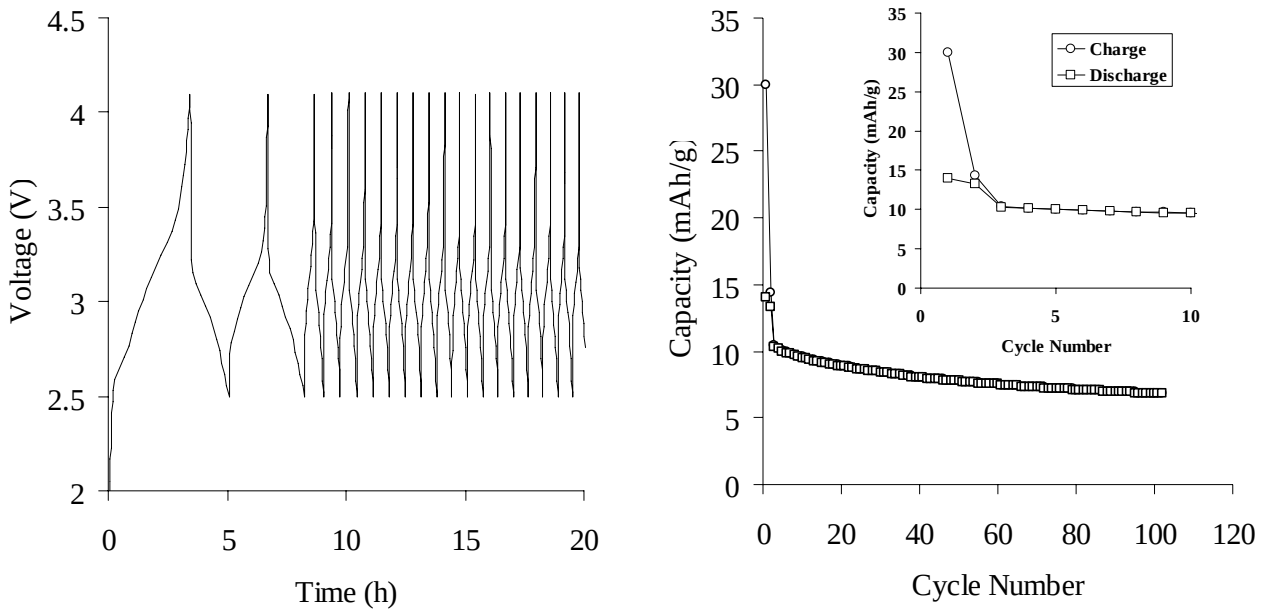

(a) (b)

Figure 6. Liquid electrolyte full cell using non-woven carbon fabric and $LiFePO_4$. (a) Voltage profile during the first 20 hours. (b) Charge and discharge curves. Inset shows a enlarged graph of cycles 1-10.

4. COMPOSITE DESIGN AND TESTING

4.1 Composite mechanics To further understand the contributions of each component to the overall mechanical performance of the composite, a simplified analysis of the structure was developed using rule of mixtures equations for composites (11). In this analysis, each layer was homogenized, or treated as possessing constant stiffness and density. The model also assumes a constant cross-sectional area with perfect bonding between layers, and only considers composite mechanical properties in a single direction. This simplified model should provide reasonable estimates of composite battery stiffness and illustrate trends in the optimization of the structure.

In the model, the composite tensile stiffness is given by

$$E_C = \frac{1}{H}\sum E_i h_i \quad , \qquad [1]$$

where E_c is the overall composite in-plane tensile stiffness, E_i is an individual ply's effective tensile stiffness, h_i is the ply thickness, H is the total composite thickness, and i numerates each ply. The density of the composite structure was calculated using a similar rule of mixtures,

$$\rho_c = \frac{1}{H}\sum \rho_i h_i \quad , \qquad [2]$$

where ρ_c represents overall composite density, and ρ_i represents each ply's density when impregnated with resin.

The general battery structure shown in Figure 3 was analyzed using this model. This composite consists of five plies: two anode plies, two separator plies, and one cathode ply. All plies utilize a polymer electrolyte matrix with a stiffness E_m of 25 MPa and a density ρ_m of 1.1 g/cm^3 (Section 2.1.1). Table 4 summarizes the material properties used for modeling the mechanical properties of these plies. The carbon fiber stiffness and density values are for 3k T-300 yarns, and the glass fiber stiffness and density values are for E-glass (11). The density for the cathode reinforcement is typical of stainless steel. The reinforcement volume fractions v_f and thicknesses are from Section 2.1. The stiffnesses for the non-woven anode and cathode reinforcements are based on the experimental measurements of Section 3, and represent overall reinforcement stiffness rather than fundamental fiber stiffness.

For the anode plies, four different configurations were considered: non-woven, unidirectional longitudinal, unidirectional transverse, and cross-ply. The unidirectional plies are intended to provide bounds on composite performance, while the cross-ply model provides a reasonable estimate for a woven fabric. For consistency, the unidirectional and cross-ply models assume a fiber volume fraction of 34%, equal to the effective volume fraction of the woven fabric from Section 2.1.2.

The unidirectional, longitudinal ply stiffness $E_{1,5}^L$ is modeled using a simple rule of mixtures:

$$E_{1,5}^L = E_m\left(1-v_f\right)+E_f v_f \quad , \qquad [3]$$

where E_f is the fiber stiffness. The unidirectional, transverse ply stiffness $E_{1,5}^T$ is calculated using the inverse rule of mixtures:

$$E_{1,5}^T = \left(\frac{1-v_f}{E_m}-\frac{v_f}{E_f}\right)^{-1} \quad . \qquad [4]$$

The cross-ply stiffness $E_{1,5}^{CP}$ is modeled as a 0°/90° stack of unidirectional composites using:

$$E_{1,5}^{CP} = \tfrac{1}{2}E^L + \tfrac{1}{2}E^T \quad . \qquad [5]$$

In this equation, the cross-ply laminate has the same thickness, carbon fiber, and fiber volume fraction as our woven fabric. The calculated stiffness value (39 GPa) also falls within the trends reported by Naik for similar woven fabrics (12). Note that this cross-ply model will likely overestimate the properties of a true woven composite, in which the undulating crimp of the fibers reduces their mechanical efficiency by ~ 20-50% (12).

Table 4. Material parameters used for composite laminate analysis. E_i is the calculated stiffness of each ply.

Ply	**Function**	**Reinforcement**	h (mm)	ρ_f (g/cm^3)	v_f (%)	E_f (GPa)	E_i (GPa)
1, 5	Anode	Uni. or cross-ply carbon fiber	0.33	1.8	34	231	39
1, 5	Anode	Non-woven carbon fiber	0.25	1.8	7.6	2.5*	2.5
2, 4	Separator	Cross-ply glass fiber	0.11	2.5	35	72	13
3	Cathode	Perforated stainless steel	0.05-0.45	8.0	45	20.5*	20.5

* Values for effective reinforcement stiffness

Modeling of the non-woven fabric anode is complicated by the fact that a non-woven composite cannot, in general, be accurately modeled using simple rule-of-mixtures. However, since the electrolyte matrix is very soft compared to the reinforcement (Table 4), we can reasonably assume that the non-woven ply stiffness $E_{1,5}^{NW}$ is equal to the measured reinforcement stiffness alone (2.5 GPa).

The cathode reinforcement, a perforated foil, also cannot be accurately modeled using simple rule of mixtures. However, as in the case of the non-woven fabric, the high stiffness of the cathodic substrate relative to the matrix allows us to assume that the cathode ply stiffness E_3 is equal to the measured perforated foil stiffness alone (20.5 GPa). Also note that, for this study, the overall composite stiffness is calculated as cathode thickness varies from 0.05 - 0.45 mm. A full exploration of the effect of various component thicknesses will be presented in a future publication.

The separator reinforcement is a woven glass fabric that is modeled using the cross-ply calculation of Eqn. 5 and the glass fiber volume fraction and stiffness values from Table 4. Equation 5 produces a tensile stiffness of 13 GPa for the glass separator ply.

All ply densities ρ_i are calculated using the rule of mixtures

$$\rho_i = \rho_m\left(1 - v_f\right) + \rho_f v_f \quad , \qquad [6]$$

where the reinforcement densities are given in Table 4.

Figure 7 shows the resulting composite specific stiffness, E_c/ρ_c, for a range of anode configurations and cathode thicknesses. The model predicts a large increase in composite battery in-plane specific stiffness for woven fabrics (as represented by the cross-ply model) over non-woven fabrics. This trend is expected since the woven carbon fabric has a higher fiber volume fraction than the non-woven fabric. In this case, half of the fibers in the woven fabric are aligned with the loading direction, as opposed to a smaller fraction of the fibers in the non-woven fabric. This difference in fiber orientation contributes to the difference in tensile stiffness between the woven and non-woven fabrics. Since the cathode substrate has a lower specific stiffness than carbon and glass fiber, the specific in-plane tensile stiffness of the composite battery decreases as the thickness of the cathode substrate increases. According to the *Designers, Specifiers and Buyers Handbook for Perforated Metals* (13), the elastic modulus of a perforated metal decreases almost linearly as hole size and open surface area increases. The density, and thus specific stiffness, also decrease linearly with increasing hole size and open surface area. Therefore, regardless of perforation scheme, the thickness of the metal cathode ply should be minimized or replaced with a material of higher specific stiffness in order to maximize the in-plane specific stiffness of the entire composite.

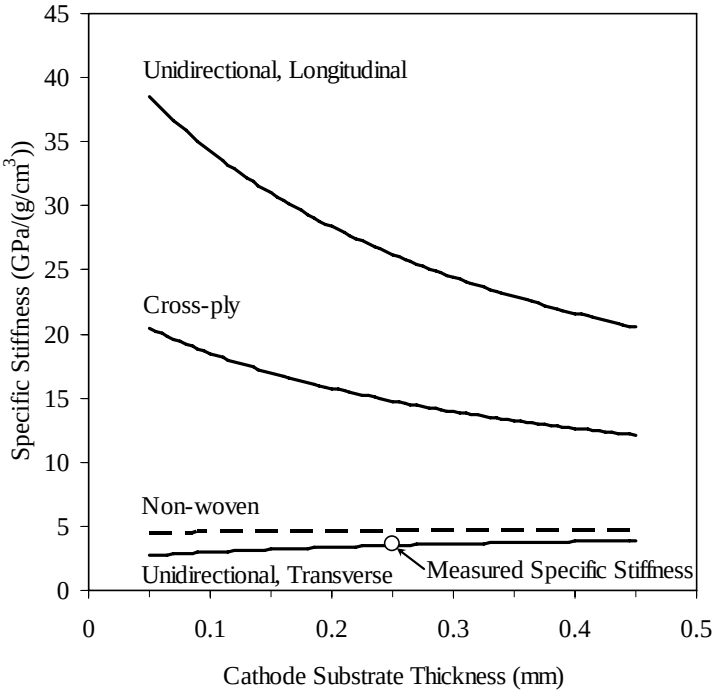

Figure 7. Calculated composite battery specific tensile stiffness vs. cathode substrate thickness. Each line represents a different type of carbon fabric used in the model. The data point represents the measured composite stiffness from Section 4.2.

4.2 Composite mechanical properties Figure 8 shows a plot of the typical tensile behavior of the composite samples. All of the samples behaved and failed in the same manner. Figure 9 shows a failed battery tensile sample. At peak load, the perforated steel failed and the load dropped to about 1/3 of the maximum value. The steel failure was audible, and visual inspection after testing confirmed this failure as shown in Figure 9. After the steel failed, the load remained constant as the strain briefly increased. During this short plateau, the glass fabric appeared to sustain most of the load, and failed shortly after the steel failure. As with the steel, the glass fabric failure was audible, and the failure location was visible after the test. The carbon fabric never failed, indicating that the load was not effectively transferred into the carbon fabric. If the load was properly distributed in the samples and the matrix provided complete adhesion and load transfer, the carbon fabric should fail first since it cannot sustain as much strain as the stainless steel and glass fabric. The observed behavior can be attributed to a number of material or test configuration issues: poor fiber-matrix interface, low matrix stiffness and/or strength in combination with insufficient end tab length, or insufficient sample size. The average, measured specific tensile stiffness for these composites is plotted in Figure 7. The measured specific stiffness is 3.6 GPa/(g/cm^3), while theory predicts a specific stiffness of about 14.6 GPa/(g/cm^3) for a cross-ply carbon fiber fabric and 0.25-mm-thick cathode. Some of this difference can be attributed to the reduced efficiency of a true woven fabric, as compared to our cross-ply model assumption (12). However, this discrepancy also evidences incomplete load transfer into the carbon fabric, which would greatly contribute to the overall composite stiffness under ideal conditions. Better fabrication methods are currently under investigation to improve adhesion and wetting of the resin to the fibers and will be reported in a future publication.

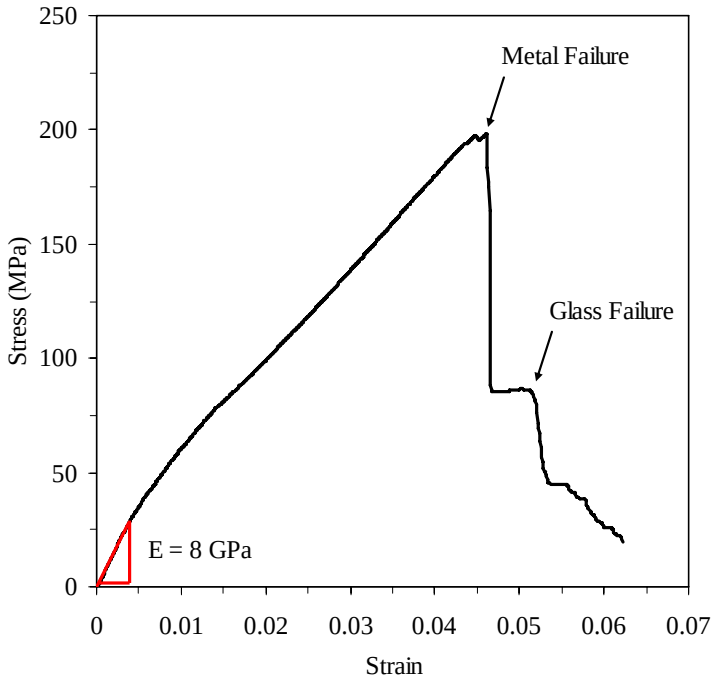

Figure 8. Typical stress vs. strain plot for a structural composite battery in tension.

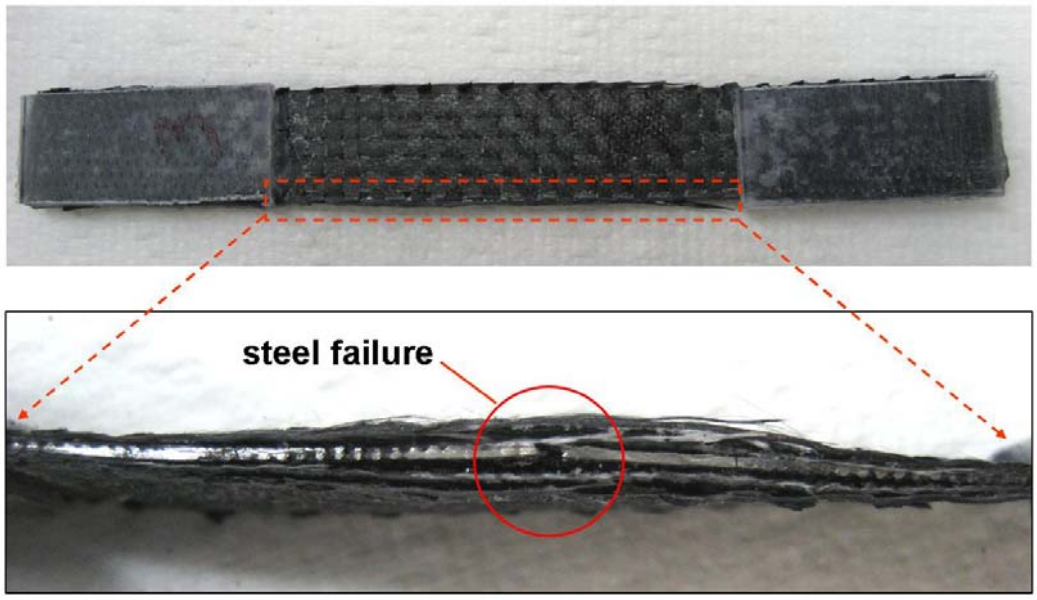

Figure 9. A failed composite battery tensile specimen.

4.3 Composite electrochemical properties The resistances of both batteries constructed for electrochemical testing were found to be very low. The composite battery with the woven anode had a resistance of 4.5 ohms, and the composite battery with the non-woven anode had a resistance of 8.4 ohms. There are a number of possible sources of electrical leakage. One possibility is that the electrolyte itself permits electron transport. However, this scenario is unlikely, as resistivity measurements on the candidate electrolyte material have typically shown immeasurably high electrical resistances. Another more likely possibility is that the separator layer was compromised, allowing direct anode-to-cathode contact. However, previous experiments also have shown that the separator is a robust and effective barrier to anode and cathode penetration. The most likely scenario is that, during VARTM resin flow, electrically conductive acetylene black particles are being separated from the cathode substrate and advected through the composite. A percolated network of these particles, even if it only forms a single conductive pathway, would result in measurable anode-to-cathode conductivity. Further investigation is underway to precisely identify the source of this electrical shorting, which will then be eliminated through modifications to our fabrication technique.

5. CONCLUSIONS

A full structural composite battery was fabricated and tested mechanically. According to our model, a woven carbon fabric anode material will produce a structural composite battery with higher specific stiffness than a composite battery utilizing a non-woven carbon anode. Tensile tests indicated that a perforated metal foil cathode substrate will produce a structural composite battery with higher specific stiffness than a woven metal mesh or expanded metal foil cathode substrate. Experimental tensile tests of a woven-carbon-fabric-anode/perforated-steel-cathode-substrate composite battery produced lower values than expected due to a weak matrix and sample dimensions. The charge and discharge capacities of the liquid electrolyte full cell were roughly equivalent with little irreversible capacity confirming that the structural electrode materials are compatible. Full structural composite batteries were made, but were unable to undergo electrochemical tests due to poor electronic insulation. Improvements to the electronic insulative properties of composite batteries are being investigated and will be addressed in future publications.

6. REFERENCES

1. J.T. South., R. H. Carter, J. F. Snyder, C. D. Hilton, D. J. O'Brien, and E. D. Wetzel., Proceedings of the 2004 MRS Fall Conference, Boston, MA, 851, (2004).
2. J.P. Thomas and M. A. Qidwai. Acta Materialia, **52**, 2155, (2004).
3. J.P. Thomas, M.A. Qidwai, JOM, **57**, 18–24, (2005).
4. J.F. Snyder, R.H. Carter, E.L. Wong, P.-A. Nguyen, K. Xu, E.H. Ngo, and E.D. Wetzel, SAMPE Fall Technical Conference Proceedings 2006. Dallas, TX, (2006).
5. J.F. Snyder, R.H. Carter, E.L. Wong, P.-A. Nguyen, K. Xu, E.H. Ngo, and E.D. Wetzel, Proceedings of the 25th Army Science Conference, (2006).
6. K. Xu. Chem. Rev., **104**, 4303, (2004).
7. N. Takami et al. J. Power Sources, **97-98**, 677, (2001).
8. G.-A. Nazri and G. Pistoia. Lithium Batteries Science and Technology. Boston, Kluwer Academic Publishers, 2004, pp. 99-102, 347-350.

9. ASTM E8-04, “Standard Test Methods for Tension Testing of Metallic Materials”, ASTM International. 2007.
10. R. Fong, U. von Sacken, J. R.Dahn. J. Electrochem. Soc., **137**, 2009, (1990).
11. I. M. Daniel and O. Ishail, Engineering Mechanics of Composite Materials, Oxford University Press, New York NY, 1994, pp. 72-73, 142-184.
12. N.K. Naik, Woven Fabric Composites, Technomic Publishing, Lancaster PA, 1994, pp. 55-58.
13. Industrial Perforators Association. *Designers, Specifiers, and Buyers Handbook of Perforated Metals*. 2006. http://www.iperf.org/IPRF_DES.pdf.

7. Acknowledgements

This research was supported in part by an appointment to the Postgraduate Research Participation Program at the U.S. Army Research Laboratory administered by the Oak Ridge Institute for Science and Education through an interagency agreement between the U.S. Department of Energy and USARL.

Distribution List

ADMNSTR DEFNS TECHL INFO CTR DTIC OCP (ELECTRONIC COPY) 8725 JOHN J KINGMAN RD STE 0944 FT BELVOIR VA 22060-6218	1 elec
US ARMY RSRCH LAB IMNE ALC IMS MAIL & RECORDS MGMT AMSRD ARL D J M MILLER AMSRD ARL CI OK TL TECHL LIB (2 COPIES) AMSRD ARL CI OK T TECHL PUB (2 COPIES) 2800 POWDER MILL ROAD ADELPHI MD 20783-1197	6
US ARMY RESEARCH LAB AMSRD CI OK TP TECHL LIB ATTN T LANDFRIED APG MD 21005	1
US ARMY RESEARCH LAB AMSRD ARL WM MA J SNYDER (3 COPIES) P NGUYEN E WONG D BAECHLE AMSRD ARL WM MB R CARTER BUILDING 4600 APG MD 21005-5069	7
TOTAL	15 (1 Electronic, 14 HCs)